

**Enhancing robustness and efficiency of density matrix embedding
theory via semidefinite programming and local correlation
potential fitting**

Xiaojie Wu,¹ Michael Lindsey,² Tiangang Zhou,³ Yu Tong,¹ and Lin Lin^{1,4,*}

¹*Department of Mathematics, University of California,
Berkeley, California 94720, United States*

²*Courant Institute of Mathematical Sciences,
New York University, New York, NY 10012, United States*

³*School of Physics, Peking University, Beijing, 100871, China*

⁴*Computational Research Division, Lawrence Berkeley National Laboratory,
Berkeley, California 94720, United States*

(Dated: February 17, 2021)

Abstract

Density matrix embedding theory (DMET) is a powerful quantum embedding method for solving strongly correlated quantum systems. Theoretically, the performance of a quantum embedding method should be limited by the computational cost of the impurity solver. However, the practical performance of DMET is often hindered by the numerical stability and the computational time of the correlation potential fitting procedure, which is defined on a single-particle level. Of particular difficulty are cases in which the effective single-particle system is gapless or nearly gapless. To alleviate these issues, we develop a semidefinite programming (SDP) based approach that can significantly enhance the robustness of the correlation potential fitting procedure compared to the traditional least squares fitting approach. We also develop a local correlation potential fitting approach, which allows one to identify the correlation potential from each fragment independently in each self-consistent field iteration, avoiding any optimization at the global level. We prove that the self-consistent solutions of DMET using this local correlation potential fitting procedure are equivalent to those of the original DMET with global fitting. We find that our combined approach, called L-DMET, in which we solve local fitting problems via semidefinite programming, can significantly improve both the robustness and the efficiency of DMET calculations. We demonstrate the performance of L-DMET on the 2D Hubbard model and the hydrogen chain. We also demonstrate with theoretical and numerical evidence that the use of a large fragment size can be a fundamental source of numerical instability in the DMET procedure.

* linlin@math.berkeley.edu

I. INTRODUCTION

In order to treat strong correlation effects beyond the single-particle level for large systems, highly accurate numerical methods such as full configuration interaction (FCI) [1–3], exact diagonalization (ED) [4, 5], or the density matrix renormalization group (DMRG) [6] with a large bond dimension are often prohibitively expensive. Quantum embedding theories [7–9], such as the dynamical mean field theory (DMFT) [10–14] and density matrix embedding theory (DMET) [15–22], offer an alternative approach for treating strongly correlated systems. The idea is to partition the global system into several “impurities” to be treated accurately via a high-level theory (such as FCI/ED/DMRG), and to “glue” the solutions from all impurities via a lower-level theory. This procedure is performed self-consistently until a certain consistency condition is satisfied between the high-level and low-level theories. The self-consistency condition is particularly important when the physical system undergoes a phase transition not predicted by mean-field theory (i.e., the mean-field theory incorrectly predicts the order parameter), and quantum embedding theories provide systematic procedures to qualitatively correct the order parameter.

In this paper we focus on DMET, which has been successfully applied to compute phase diagrams of a number of strongly correlated models, such as the one-band Hubbard model both with and without a superconducting order parameter [15, 18, 23–26], quantum spin models [27, 28], and prototypical correlated molecular problems [16, 19, 29]. The self-consistency condition is usually defined so that the 1-RDMs obtained from the low-level and high-level theories match each other according to some criterion, such as matching the 1-RDM of the impurity problem [15], matching on the fragment only [16, 17], or simply matching the diagonal elements of the density matrix (i.e., the electron density) [18]. Self-consistency can be achieved by optimizing a single-body Hamiltonian, termed the correlation potential, in the low-level theory. Each optimization step requires diagonalizing a matrix, similarly to the self-consistent field (SCF) iteration step in the solution of the Hartree-Fock equations.

However, the correlation potential optimization step can become a computational bottleneck, even compared to the cost of the impurity solvers. This is because in DMET, the size of each impurity is often thought of as a constant, and therefore the cost for solving all of the impurity problems always scales linearly with respect to the global system size.

Meanwhile, the correlation potential fitting requires repeated solution of problems at the single-particle level and is closely related to the density inversion problem [30, 31]. In order to evaluate the derivative, the computational effort is similar to that of a density functional perturbation theory (DFPT) calculation [32]. The number of iterations to optimize the correlation potential can also increase with respect to the system size, especially for gapless systems, provided the procedure can converge at all.

In this paper, we propose two improvements to significantly increase the efficiency and the robustness of the correlation potential fitting procedure. To enhance the robustness, we propose to reformulate the correlation potential fitting problem as a semidefinite program (SDP). It is theoretically guaranteed that when the correlation potential is uniquely defined, it coincides with the optimal solution of the SDP. Moreover, as a convex optimization problem, the SDP has no spurious local minima. To improve the efficiency, we introduce a local correlation potential fitting approach. The basic idea is to perform local correlation potential fitting on each impurity to match the high-level density matrix and the local density matrix. Then the local correlation potentials are patched together to yield the high-level density matrix. We may further combine the two approaches and utilize the SDP reformulation for each impurity. This approach is dubbed local-fitting based DMET (L-DMET). We prove that the results obtained from DMET and L-DMET are equivalent. Nonetheless, L-DMET scales linearly with respect to the system size in each iteration of DMET. It is numerically observed that L-DMET does not require more iterations than DMET. This is particularly advantageous for the simulation of large systems.

The rest of the paper is organized as follows. In Section II, we first briefly present the formulation of DMET. In particular, DMET can be concisely viewed from a linear algebraic perspective using the CS decomposition. The SDP reformulation of the correlation potential fitting is introduced in Section III as an alternative approach to the least squares problem in DMET. In Section IV, we present the local correlation fitting approach (L-DMET) and show the equivalence between the fixed points of DMET and L-DMET. The relation between the current work and a few related works, such as the finite temperature generalization and the p-DMET [33], is discussed in Section V. Numerical results for the 2D Hubbard model and the hydrogen chain are given in Sections VI and VII, respectively. We conclude in Section VIII. The proofs of the propositions in the paper are given in the appendices.

II. BRIEF REVIEW OF DMET

Consider the problem of finding the ground state of the quantum many-body Hamiltonian operator in the second-quantized formulation

$$\hat{H} = \hat{t} + \hat{v}^{\text{ee}} = \sum_{pq}^L t_{pq} \hat{a}_p^\dagger \hat{a}_q + \frac{1}{2} \sum_{pqrs}^L (pr|qs) \hat{a}_p^\dagger \hat{a}_q^\dagger \hat{a}_s \hat{a}_r. \quad (1)$$

Here L is the number of spin orbitals. The corresponding Fock space is denoted by \mathcal{F} , which is of dimension 2^L . The number of electrons is denoted by N_e . We partition the L sites into N_f fragments. Without loss of generality, we assume each fragment has the same size L_A , though a non-uniform partition is possible as well. We define the set of block-diagonal matrices with the sparsity pattern corresponding to the fragment partitioning as

$$\mathcal{S} = \left\{ A = \bigoplus_{x=1}^{N_f} A_x \mid A_x \in \mathbb{C}^{L_A \times L_A}, A_x = A_x^\dagger \text{ for } x = 1, \dots, N_f \right\}, \quad (2)$$

where \bigoplus indicates the direct sum of matrices, i.e.

$$\bigoplus_{x=1}^{N_f} A_x = \begin{pmatrix} A_1 & 0 & \cdots & 0 \\ 0 & A_2 & \cdots & 0 \\ \vdots & \vdots & \ddots & \vdots \\ 0 & 0 & \cdots & A_{N_f} \end{pmatrix}.$$

Density matrix embedding theory (DMET) can be formulated in a self-consistent manner with respect to a *correlation potential* $u \in \mathcal{S}$. For a given u , the low-level (also called the single-particle level) Hamiltonian takes the form

$$\hat{H}^{\text{ll}}(u) = \hat{f} + \hat{c}(u). \quad (3)$$

Here $\hat{c}(u) = \sum_{pq} u_{pq} \hat{a}_p^\dagger \hat{a}_q$ is a quadratic interaction associated with the correlation potential. When the ground state of \hat{H}^{ll} can be uniquely defined, this ground state is a single-particle Slater determinant denoted by $|\Psi^{\text{ll}}(u)\rangle$, given by a matrix $C \in \mathbb{C}^{L \times N_e}$. The associated low-level density matrix is denoted by $D^{\text{ll}}(u) := CC^\dagger$. Here $\hat{f} := \sum_{pq} f_{pq} \hat{a}_p^\dagger \hat{a}_q$ is given by a fixed matrix f . The simplest choice is $f = t$, but other choices are possible as well [19]. Then the low-level density matrix can be expressed as $D^{\text{ll}}(u) = \mathcal{D}(f + u, N_e)$, which is well-defined when the matrix $f + u$ has a positive gap between the (N_e) -th and $(N_e + 1)$ -th eigenvalues. (Note that throughout we shall use the general notation $\mathcal{D}(h, N)$ to denote the N -particle

density matrix induced by the non-interacting Hamiltonian specified by the single particle matrix h .)

For each fragment x , the Schmidt decomposition of the Slater determinant $|\Psi^{\text{ll}}(u)\rangle$ can be used to identify a certain subspace $\mathcal{F}_x \subset \mathcal{F}$ that contains $|\Psi^{\text{ll}}(u)\rangle$ as follows. Without loss of generality, we assume the fragment x consists of first L_A orbitals labeled by $\{1, 2, \dots, L_A\}$. Since C has orthonormal columns as $C^\dagger C = I_{N_e}$, we may apply the CS decomposition [34, 35] and obtain

$$C = \begin{pmatrix} U_A \Sigma_A V^\dagger \\ U_B \Sigma_B V^\dagger + U_{\text{core}} V_\perp^\dagger \end{pmatrix}. \quad (4)$$

Here $U_A \in \mathbb{C}^{L_A \times L_A}$, $U_B \in \mathbb{C}^{(L-L_A) \times L_A}$, $U_{\text{core}} \in \mathbb{C}^{(L-L_A) \times (N_e - L_A)}$, $V \in \mathbb{C}^{N_e \times L_A}$ and $V_\perp \in \mathbb{C}^{N_e \times (N_e - L_A)}$ are all column orthogonal matrices. $\Sigma_A, \Sigma_B \in \mathbb{C}^{L_A \times L_A}$ are non-negative, diagonal matrices and they satisfy $\Sigma_A^2 + \Sigma_B^2 = I_{N_e}$. Furthermore, $U_B^\dagger U_{\text{core}} = 0$, $V^\dagger V_\perp = 0$. The CS decomposition (4) defines a low-level density matrix. On the other hand, the decomposition as well as $U_A, U_B, U_{\text{core}}$ can be deduced from D^{ll} directly. The relation is given in Appendix B.

Throughout the paper, we assume the following condition is satisfied.

Assumption 1 *We assume $N_e > L_A$, and for each fragment x , the diagonal entries of Σ_A, Σ_B in Eq. (4) are not 0 or 1.*

When Assumption 1 is violated, particularly when L_A is large relative to N_e (such as in the context of a large basis set), the choice of the correlation potential is generally not unique (Appendix A).

The decomposition (4) allows us to define the fragment, bath and core orbitals as the columns of

$$\Phi_x^{\text{frag}} = \begin{pmatrix} I_{L_A} \\ 0 \end{pmatrix}, \quad \Phi_x^{\text{bath}} = \begin{pmatrix} 0 \\ U_B \end{pmatrix}, \quad \Phi_x^{\text{core}} = \begin{pmatrix} 0 \\ U_{\text{core}} \end{pmatrix}.$$

In particular, the number of bath orbitals is only L_A . This is a key observation in DMET [15, 16]. The rest of the single-particle orbitals orthogonal to $\Phi_x^{\text{frag}}, \Phi_x^{\text{bath}}, \Phi_x^{\text{core}}$ are called the virtual orbitals and are denoted by

$$\Phi_x^{\text{vir}} = \begin{pmatrix} 0 \\ U_{\text{vir}} \end{pmatrix}.$$

The virtual orbitals are not explicitly used in DMET. We also define the set of impurity orbitals, which consists of fragment and bath orbitals, as

$$\Phi_x = \begin{pmatrix} \Phi_x^{\text{frag}} & \Phi_x^{\text{bath}} \end{pmatrix} = \begin{pmatrix} I_{L_A} & 0 \\ 0 & U_B \end{pmatrix}.$$

Using a canonical transformation, the fragment, bath, core and virtual orbitals together allow us to define a new set of creation and annihilation operators $\{\hat{c}_p^\dagger, \hat{c}_p\}$ in the Fock space satisfying several properties. First, $\hat{c}_1^\dagger, \dots, \hat{c}_{L_A}^\dagger$ correspond exactly to \hat{a}_p^\dagger for all p in the fragment x . Second, the operators $\hat{c}_1^\dagger, \dots, \hat{c}_{2L_A}^\dagger$ generate an active Fock space $\mathcal{F}_x^{\text{act}}$ of dimension 2^{2L_A} , such that the low-level wavefunction can be written as $|\Psi^{\text{ll}}(u)\rangle = |\Psi_x^{\text{act}}(u)\rangle \otimes |\Psi_x^{\text{inact}}(u)\rangle$, where $|\Psi_x^{\text{inact}}(u)\rangle$ lies in the inactive space generated by $c_{2L_A+1}^\dagger, \dots, c_{N_e}^\dagger$ corresponding to the core orbitals (the virtual orbitals do not contribute to the Slater determinant $|\Psi^{\text{ll}}(u)\rangle$). Then the subspace \mathcal{F}_x , called the x -th impurity space, can be defined by

$$\mathcal{F}_x = \{|\Psi\rangle \otimes |\Psi_x^{\text{inact}}(u)\rangle : |\Psi\rangle \in \mathcal{F}_x^{\text{act}}\}.$$

Evidently $|\Psi^{\text{ll}}(u)\rangle \in \mathcal{F}_x \simeq \mathcal{F}_x^{\text{act}}$. Then by a Galerkin projection onto \mathcal{F}_x [19], one derives a ground-state quantum many-body problem on each of the active spaces $\mathcal{F}_x^{\text{act}}$, specified by an impurity Hamiltonian (or embedding Hamiltonian) of the following form:

$$\hat{H}_x^{\text{emb}} = \hat{t}_x + \hat{v}_x^{\text{emb}} + \hat{v}_x^{\text{ee,emb}} - \mu \hat{N}_x^{\text{frag}}. \quad (5)$$

Here \hat{t}_x is a single-particle operator specified by the active-space block of the canonically transformed single-particle matrix t , $\hat{v}_x^{\text{ee,emb}}$ is a two-particle interaction specified by the active-space block of the canonically transformed two-particle tensor $(pr|qs)$, and \hat{v}_x^{emb} is an additional single-particle operator due to the core electron wavefunction $|\Psi_x^{\text{inact}}(u)\rangle$ in the inactive space. Finally, \hat{N}_x^{frag} is the total number operator for the fragment part of the x -th impurity, and μ is a scalar determined by a criterion to be discussed below.

Given Assumption 1, the number of core orbital electrons in $|\Psi_x^{\text{inact}}(u)\rangle$ is $N_e - L_A$, so the number of electrons in the active space of each impurity is equal to L_A . Let $D_x^{\text{hl}} \in \mathbb{C}^{2L_A \times 2L_A}$ be the single-particle density matrix corresponding to the L_A -particle ground state of the many-body Hamiltonian H_x^{emb} , so $\text{Tr}[D_x^{\text{hl}}] = L_A$. Define the matrix $E = (I_{L_A} \quad 0_{L_A \times L_A})^\top$, so the upper-left block of the density matrix D_x^{hl} , corresponding to the fragment, can be written as $D_x^{\text{hl,frag}} := E^\top D_x^{\text{hl}} E$. Going through all fragments, we obtain the diagonal matrix

blocks of the high-level density matrix as

$$D^{\text{hl,frag}} := \bigoplus_{x=1}^{N_f} D_x^{\text{hl,frag}} \in \mathcal{S}. \quad (6)$$

However, the total number of electrons from all fragments must still be equal to N_e . This requires the following condition to be satisfied

$$\text{Tr}[D^{\text{hl,frag}}] = \sum_{x=1}^{N_f} \text{Tr}(D_x^{\text{hl,frag}}) = N_e. \quad (7)$$

Eq. (7) is achieved via the appropriate choice of the Lagrange multiplier (i.e., chemical potential) μ in the definition (5) of the embedding Hamiltonian.

Once the matrix blocks in $D^{\text{hl,frag}}$ are obtained, DMET adjusts the correlation potential by solving the following least squares problem

$$\min_{u \in \mathcal{S}^0} \sum_{x=1}^{N_f} \|D_x^{\text{hl,frag}} - (\Phi_x^{\text{frag}})^\dagger \mathcal{D}(f + u, N_e) \Phi_x^{\text{frag}}\|_F^2. \quad (8)$$

Here $(\Phi_x^{\text{frag}})^\dagger \mathcal{D}(f + u, N_e) \Phi_x^{\text{frag}}$ gives the the diagonal matrix block corresponding to the x -th fragment. We define $\mathcal{S}^0 := \{A \in \mathcal{S} \mid \text{Tr}[A] = 0\}$, and the traceless condition is added due to the fact that adding a constant in the diagonal entries of u does not change the objective function. The minimization problem (8) can be solved with standard nonlinear optimization solvers such as the conjugate gradient method or the quasi-Newton method, and the gradient of the objective function with respect to u can be analytically calculated [19].

Finally, in order to formulate the DMET self-consistent loop, we define the nonlinear mapping $\mathfrak{D} : u \mapsto D^{\text{hl,frag}}$. This mapping takes the correlation potential u as the input, generates the bath orbitals, and solves all impurity problems to obtain the matrix blocks $D^{\text{hl,frag}}$. We also define the mapping $\mathfrak{F} : D^{\text{hl,frag}} \mapsto u$, which takes the high-level density matrix blocks $D^{\text{hl,frag}}$ as the input and updates the correlation potential. Formally, the self-consistency condition of DMET can be formulated as

$$u = \mathfrak{F} \circ \mathfrak{D}(u). \quad (9)$$

In the discussion above, the definition of the mapping \mathfrak{F} and the well-posedness of the nonlinear fixed point problem hinges on the uniqueness of the solution of Eq. (8). In Appendix A we show that the condition $N_e \geq L_A$ as in Assumption 1 is a necessary condition for the correlation potential to be uniquely defined. The practical consequences of this assumption will also be studied in Section VII.

III. ENHANCING THE ROBUSTNESS: SEMIDEFINITE PROGRAMMING

In order to improve the robustness of correlation potential fitting, we develop an alternative approach to the least squares approach in Eq. (8). Consider a mapping $F : \mathcal{S} \rightarrow \mathbb{R}$ defined by

$$F(u) = \mathcal{E}_{N_e}[f + u],$$

where \mathcal{E}_{N_e} gives the sum of the lowest N_e eigenvalues of the matrix $f + u$. Note that \mathcal{E}_{N_e} is a concave function, and F is a composition of a concave function with a linear function. Hence F is a concave function on \mathcal{S} . However, F is not smooth: there are singular points where $f + u$ is gapless, i.e., there is no gap between the (N_e) -th and $(N_e + 1)$ -th eigenvalues.

Whenever a matrix A is gapped, we have $\nabla_A \mathcal{E}_{N_e}(A) = \mathcal{D}(A, N_e)$. This is in fact a slight generalization of the Hellmann-Feynman theorem, which is precisely the case when $N_e = 1$. Therefore $\nabla_{u_x} F(f + u) = (\Phi_x^{\text{frag}})^\dagger \mathcal{D}(f + u, N_e) \Phi_x^{\text{frag}}$ whenever $f + u$ is gapped.

The correlation potential fitting problem requires us to evaluate the inverse of the gradient mapping $\nabla_u F = \bigoplus_{x=1}^{N_f} \nabla_{u_x} F$ at the point $D^{\text{hl,frag}}$. Since F is concave, the inverse mapping relates to the gradient of the concave conjugate, or the Legendre-Fenchel transform [36]. The conjugate is denoted by $F^* : \mathcal{S} \rightarrow \mathbb{R}$ and defined as

$$F^*(P) = \inf_{u \in \mathcal{S}^0} \left\{ \sum_{x=1}^{N_f} \text{Tr}[P_x u_x] - F(u) \right\}, \quad P \in \mathcal{S}. \quad (10)$$

Here we use the new notation P to denote a generic block diagonal matrix that may not be the same as $D^{\text{hl,frag}}$. Again we may restrict u to be within the set \mathcal{S}^0 since the objective function of Eq. (10) is invariant under the transformation $u \leftarrow u + \mu I$. In fact, the minimization problem in Eq. (10) is a slightly generalized formulation of the variational approach for finding the optimal effective potential (OEP)[30, 31], as well as the Lieb approach for finding the exchange-correlation functional [37]. We will show:

Proposition 2 *Suppose $0 \prec D_x^{\text{hl,frag}} \prec I_{L_A}$ for $x = 1, \dots, N_f$ and $\sum_{x=1}^{N_f} \text{Tr}[D_x^{\text{hl,frag}}] = N_e$. Then the convex optimization problem for the evaluation of $F^*(D^{\text{hl,frag}})$, i.e., the optimization problem in Eq. (10) where $P = D^{\text{hl,frag}}$, admits an optimizer u^* . Then $D^{\text{hl,frag}}$ lies in the supergradient set of F at u^* . If $f + u^*$ has a gap between its (N_e) -th and $(N_e + 1)$ -th eigenvalues (ordered increasingly), then $\mathcal{D}(f + u^*, N_e)$ has diagonal blocks matching $D^{\text{hl,frag}}$, i.e., we achieve exact fitting. If $f + u^*$ has no gap, then the ground state and the mapping*

$\mathcal{D}(f + u^*, N_e)$ are ill-defined, and, assuming that the optimizer u^* is unique, there is no correlation potential u that yields a well-defined low-level density matrix achieving exact fitting.

The proof of Proposition 2 is provided in Appendix C. We remark that the matter of whether there exists a *unique* optimizer $u^* \in \mathcal{S}^0$ appears to be subtle. Such uniqueness would follow from the strict concavity of $\mathcal{F}|_{\mathcal{S}^0}$, if it could be established.

Now we further demonstrate that the convex optimization problem of Proposition 2 can be equivalently reformulated as a semidefinite program (SDP), which can be tackled numerically by standard and robust solvers. The equivalence is established by the following proposition, and the proof is in Appendix D.

Proposition 3 *Optimizers u^* as in Proposition 2 can be obtained from optimizers (u^*, Z^*, α^*) of the semidefinite program*

$$\begin{aligned} & \underset{u \in \mathcal{S}^0, Z \in \mathbb{C}^{L \times L}, \alpha \in \mathbb{R}}{\text{minimize}} && \sum_{x=1}^{N_f} \text{Tr}[D_x^{\text{hl,frag}} u_x] - \alpha N_e + \text{Tr}(Z) \\ & \text{subject to} && f + u + Z - \alpha I \succeq 0 \\ & && Z \succeq 0. \end{aligned} \tag{11}$$

The minimization problem (11) appears to be significantly different from standard problems in electronic structure calculation. However, we may verify that if u^* is a minimizer and $f + u^*$ is gapped with the standard eigenvalue decomposition

$$(f + u^*)\psi_k = \lambda_k \psi_k,$$

then α is a chemical potential satisfying $\lambda_{N_e} < \alpha < \lambda_{N_e+1}$, and $Z = \sum_{i=1}^{N_e} (\alpha - \lambda_i) \psi_i \psi_i^\dagger$. Then $Z \succeq 0$, $f + u^* + Z - \alpha I = \sum_{a=N_e+1}^L (\lambda_a - \alpha) \psi_a \psi_a^\dagger \succeq 0$, and the objective function of Eq. (11) is indeed equal to $\sum_{x=1}^{N_f} \text{Tr}[D_x^{\text{hl,frag}} u_x] - \sum_{i=1}^{N_e} \lambda_i = F^*(D^{\text{hl,frag}})$.

Hence, our new approach improves upon that of (8) in two ways. First, whenever exact fitting is possible, we can solve the problem with more robust optimization algorithms with strong guarantees of success and which are not, in particular, susceptible to spurious local minima. Second, whenever exact fitting is impossible, we can certify that this is indeed the case by observing that the correlation potential that we obtain defines a gapless system. By contrast, if exact fitting is not achieved in the least squares approach, it may not be possible to certify that the optimization algorithm is not merely stuck in a local minimum of the objective function.

IV. ENHANCING THE EFFICIENCY: LOCAL CORRELATION POTENTIAL FITTING

The convex optimization formulation improves the robustness of the correlation potential fitting procedure. However, we still need to solve an SDP with $(L_A + 1)L/2$ variables (the constant $1/2$ is due to the symmetry of the correlation potential), while intermediate variables such as Z can be of size $L \times L$. Hence for large inhomogeneous systems, the cost of the correlation potential fitting can be significant and may still outweigh the cost of the impurity solver. In this section, we develop a local fitting method, which decouples the global SDP problem into N_f local fitting problems, each of size $L_A \times L_A$ only. The cost of the correlation potential fitting procedure then scales linearly with respect to L , assuming the total number of iterations does not increase significantly.

The idea of performing a local fitting is motivated from the following consideration. The embedding Hamiltonian \hat{H}_x^{emb} is obtained by a Galerkin projection of \hat{H} to \mathcal{F}_x via a canonical transformation of the creation and annihilation operators. We may apply the same transformation to the low-level Hamiltonian \hat{H}^{ll} , modified by a potential v_x on the fragment, to obtain a quadratic Hamiltonian

$$\hat{H}_x^{\text{ll,emb}} = \sum_{p,q=1}^{2L_A} (\tilde{f}_x + E v_x E^\top)_{pq} c_p^\dagger c_q, \quad v \in \mathcal{S}. \quad (12)$$

Here $\tilde{f}_x = \Phi_x^\dagger (f + u) \Phi_x$ is the projected Fock matrix onto the impurity x . As before $E = (I_{L_A} \quad 0_{L_A \times L_A})^\top$, and then $E v_x E^\top \in \mathbb{C}^{2L_A \times 2L_A}$ is defined on the impurity. When $v_x = 0$, the fragment density matrix obtained from the ground state of $\hat{H}_x^{\text{ll,emb}}$ should agree with the global low-level density matrix restricted to the same fragment. (This statement will be justified in Appendix E.) Then instead of the global least squares fitting problem, we may solve a modified least squares problem

$$\min_{u \in \mathcal{S}^0} \sum_{x=1}^{N_f} \|D_x^{\text{hl, frag}} - E^\top \mathcal{D}(\tilde{f}_x + E v_x E^\top, L_A) E\|_F^2. \quad (13)$$

In contrast to Eq. (8), the minimizations with respect to different matrix blocks v_x can be performed independently, and the cost scales linearly with respect to N_f (and therefore L). Once $v := \bigoplus_{x=1}^{N_f} v_x$ is obtained, we may update the correlation potential as

$$u \leftarrow u + v = \bigoplus_{x=1}^{N_f} (u_x + v_x). \quad (14)$$

Following the discussion of Section III, we may readily formulate a convex optimization-based alternative to the least squares problem in Eq. (13). We may define the function F_x^{act} defined on the set of Hermitian $L_A \times L_A$ matrices by

$$F_x^{\text{act}}(v_x) = \mathcal{E}_{L_A} \left(\tilde{f}_x + E v_x E^\top \right).$$

Note that we do not require v_x to be traceless, since v_x is only applied to the fragment instead of the entire impurity. Then if $0 \prec D_x^{\text{hl,frag}} \prec I_{L_A}$, the convex optimization problem

$$\inf_{v_x^\dagger = v_x} \left\{ \text{Tr}[D_x^{\text{hl,frag}} v_x] - F_x^{\text{act}}(v) \right\}$$

admits a solution v_x^* . If $\tilde{f}_x + v_x^*$ has a gap between its (L_A) -th and $(L_A + 1)$ -th eigenvalues (ordered increasingly), then $\mathcal{D}(\tilde{f}_x + E v_x E^\top, L_A)$ has fragment block equal to $D_x^{\text{hl,frag}}$, i.e., we achieve exact fitting. If $\tilde{f}_x + v_x^*$ has no gap, then the ground state and 1-RDM are ill-defined, and, if the solution is unique, then there is no correlation potential v that yields a well-defined 1-RDM with exact fit. Furthermore, any optimizer v^* can be obtained from an optimizer (v^*, Z^*, α^*) of the SDP

$$\begin{aligned} & \underset{\substack{v_x \in \mathbb{C}^{L_A \times L_A}, v_x^\dagger = v_x \\ Z \in \mathbb{C}^{(2L_A) \times (2L_A)}, \alpha \in \mathbb{R}}}{\text{minimize}} & & \text{Tr}(v_x D_x^{\text{hl,frag}}) - \alpha L_A + \text{Tr}(Z) \\ & \text{subject to} & & \tilde{f}_x + E v_x E^\top + Z - \alpha I \succeq 0, \\ & & & Z \succeq 0. \end{aligned} \tag{15}$$

In the following discussion, the procedure above will be referred to as the local-fitting based DMET (L-DMET), which combines local correlation potential fitting and semidefinite programming. Note that DMET and L-DMET solve fixed-point problems of the same form (9), but with different choices of mappings \mathfrak{F} . We define the mappings associated with DMET and L-DMET as $\mathfrak{F}^{\text{DMET}}$ and $\mathfrak{F}^{\text{L-DMET}}$, respectively. As stated precisely in Proposition 4 below, the fixed points of L-DMET and DMET are equivalent. Hence L-DMET introduces no loss of accuracy relative to DMET. The proof is given in Appendix E.

Proposition 4 *Suppose Eq. (9) has a fixed point u^* with $\mathfrak{F} = \mathfrak{F}^{\text{DMET}}$, and $f + u^*$ has a gap between its (N_e) -th and $(N_e + 1)$ -th eigenvalues (ordered increasingly). Let $D_x^{\text{hl,frag}} \in \mathcal{S}$ be the associated high-level density matrix blocks, which satisfy $0 \prec D_x^{\text{hl,frag}} \prec I_{L_A}$ for $x = 1, \dots, N_f$ and $\text{Tr}[D_x^{\text{hl,frag}}] = N_e$. Then u^* is a fixed point of Eq. (9) with $\mathfrak{F} = \mathfrak{F}^{\text{L-DMET}}$. Similarly, under the same assumptions, if u^* is a fixed point of L-DMET, then it is also a fixed point of DMET.*

In summary, L-DMET only leads to a modular modification of an existing DMET implementation. We provide a unified pseudocode for DMET and L-DMET in Algorithm 1.

Algorithm 1 A unified pseudocode of DMET and L-DMET.

Input: Initial low level density matrix $D^{\text{ll},(0)}$, and chemical potential $\mu^{(0)}$.

Partition the system into N_f fragments.

Output: Correlation potential u and high-level density matrix blocks $D^{\text{hl,frag}}$

```

1: while correlation potential  $u^{(k)}$  has not converged do
2:   Solve the ground state associated with  $\hat{H}^{\text{ll}} = \hat{f} + \hat{c}(u^{(k)})$  for  $D^{\text{ll},(k)}$ 
3:   for  $x$  in  $1, \dots, N_f$  do
4:     Compute bath orbitals for impurity  $x$ .
5:   end for
6:   Set  $m = 0, \nu^{(m)} = \mu^{(k)}$ 
7:   while chemical potential  $\nu^{(m)}$  has not converged do
8:     for  $x$  in  $1, \dots, N_f$  do
9:       Solve the impurity problem  $\hat{H}_x^{\text{emb}} - \nu^{(m)} \hat{N}_x^{\text{frag}}$  for  $D_x^{\text{hl,frag}}$ .
10:    end for
11:    Use  $\text{Tr}(D^{\text{hl,frag}})$  to update the chemical potential to  $\nu^{(m+1)}$ .
12:    Set  $m \leftarrow m + 1$ .
13:  end while
14:  Set  $\mu^{(k+1)} = \nu^{(m)}$ .
15:  if DMET then
16:    Update  $u^{(k+1)}$  by solving the global correlation potential fitting problem.
17:  end if
18:  if L-DMET then
19:    Update  $u^{(k+1)}$  by solving the local correlation potential fitting problem.
20:  end if
21:  Set  $k \leftarrow k + 1$ .
22: end while

```

V. OTHER CONSIDERATIONS

A related approach to improve the efficiency of the correlation potential fitting is called projected-based DMET (p-DMET) [33], which directly finds the closest low-level density matrix D^{ll} to the entire high-level density matrix D^{hl} , subject to rank- N_e constraints. This completely eliminates the correlation potential fitting procedure and is very efficient for large systems. It also eliminates the uncertainty introduced by the uniqueness of the correlation potential. However, it has also been observed that the result of the p-DMET has a stronger initial state dependence than DMET. In particular, when p-DMET is used to study the phase diagrams of a 2D Hubbard model, the resulting phase boundary from p-DMET is blurrier than that obtained from DMET [33]. On the other hand, Proposition 4 guarantees that the fixed points of L-DMET and DMET are the same. We will also demonstrate by numerical results that L-DMET and DMET can produce identical phase diagrams.

When the two-body interaction term ($pr|qs$) is nonlocal (such as in the case of quantum chemistry calculations), one often replaces \hat{f} in Eq. (3) by $\hat{f} = \hat{f}(D^{\text{ll}})$, which is a Fock operator that depends on the low-level density matrix D^{ll} . Then Eq. (3) needs to be solved self-consistently as in the case of solving Hartree-Fock equations. Such an extra self-consistency step at the low level is also called *charge self-consistency* [20] and can be used to take into account long-range interactions beyond the sparsity pattern of \mathcal{S} .

When $f + u^*$ is gapless, the corresponding low-level density matrix D^{ll} is ill-defined (even though u^* itself may still be well-defined via the semidefinite programming formulation of correlation potential fitting), and the self-consistent iteration of Eq. (9) cannot proceed without modification. One possibility is to use the recently developed finite temperature DMET [21]. The other possibility is to generate a mixed-state low-level density matrix using a Fermi-Dirac smearing with a low temperature, and extract the bath orbitals from the density matrix directly (see Appendix B). We remark that both options formally violate the original premise of DMET, namely the Schmidt decomposition of a Slater determinant [15, 16] or the CS decomposition as in Eq. (4). A proper treatment of gapless systems remains a future research direction.

VI. NUMERICAL EXPERIMENTS: 2D HUBBARD MODEL

The 2D Hubbard model can describe rich physical phenomena including phase transitions [38], superconductivity [24], charge and spin density waves [39, 40], stripe order [26, 41], etc. Here we report the performance of L-DMET for the 2D Hubbard model on a square lattice with periodic boundary conditions.

The fragment size is set to 2×2 . The initial guess and the low-level density matrix are generated by the unrestricted Hartree Fock (UHF) method. When the system becomes gapless, we use Fermi-Dirac smearing with $\beta = 100$ (i.e., temperature $T = 0.01$ in the unit of the hopping parameter $t = 1$) according to the discussion in Section V. The finite temperature smearing in zero-temperature DMET is a numerical regularization technique. Smaller choices for β correspond to more severe regularization and reduced accuracy in the solution of DMET. In fact, in order to improve numerical convergence in of the least squares fitting procedure (8), we *always* to add a temperature (always set to $T = 0.01$) within the fitting procedure itself. Hence we in fact solve (8) where the map \mathcal{D} is understood to indicate the appropriate density matrix at temperature $T = 0.01$. The bath orbitals are then extracted from the resulting finite-temperature density matrix via the same approach as described above.

The impurity problems are solved by full configuration interaction (FCI) implemented in PySCF. The number of orbitals in each impurity problem is fixed to be 8 orbitals. We present results for both DMET and L-DMET. Within DMET we solve the least squares problem (8) using BFGS via SciPy, and within L-DMET we solve the SDP (15) with a splitting conic solver (SCS)[42, 43] called via CVXPY [44, 45]. For both of the methods, the convergence tolerance is set to be 10^{-8} . The convergence criterion of the DMET and L-DMET fixed point problem is set to

$$\frac{|E^{(k)} - E^{(k+1)}|}{|E^{(k)}|} < 10^{-8} \quad \text{and} \quad \frac{\|D^{\text{hl},(k)} - D^{\text{hl},(k+1)}\|_F}{\|D^{\text{hl},(k)}\|_F} < 10^{-6}. \quad (16)$$

A. Comparison of semidefinite programming and least squares fitting

Before presenting an overall comparison of DMET and L-DMET, we first present a comparison of the two approaches to the global correlation potential fitting procedure presented above, namely the least squares approach (8) (interpreted at finite temperature $T = 0.01$

to improve numerical convergence, as discussed above) and the SDP approach (11). Our results in this section compare these two approaches for the *first* correlation potential fitting step of DMET, initialized from UHF on the 6×6 2D Hubbard model.

We measure the success rates of the two methods as follows. For a given on-site interaction strength U and filling factor n (i.e., the number of electrons divided by the number of sites), the success rate is defined as

$$\text{success rate} = \frac{\text{number of successful samples}}{\text{number of total samples}} \quad (17)$$

Each sample is specified by a random potential (each entry of which is sampled independently from the uniform distribution $\mathcal{U}[-0.1, 0.1]$), which is added to the one-body Hamiltonian. The total number of samples is 1000. The least squares method fails if the norm of the gradient is greater than 10^{-8} after 2000 iterations. The SDP method fails if any of the primal residual, the dual residual and the duality gap is greater than 10^{-9} after 2500 steps. The success rate is measured for multiple values of both U and n .

Fig. 1 shows that semidefinite programming is much more robust than the least squares approach, despite the fact that the least squares fitting is performed with some finite temperature smearing. The least squares procedure can reliably converge only when the number of electrons is 18 and 26. Typically, the least squares approach is robust at half-filling without a random potential. However, when the random potential is added, the least squares approach fails frequently. On the other hand, the SDP method succeeds consistently across most test cases. The lowest success rate of the SDP method (around 90%) occurs near $U = 6.0$ at half-filling. The success rate is nearly 100% in all other cases.

We summarize the results for the correlation potential fitting as follows: as a regularization technique, the finite temperature smearing can improve the robustness of the least squares approach in the gapless case. However, the regularized problem may still be ill-conditioned to solve using solvers such as BFGS. On the other hand, the SDP approach is parameter-free. The numerical tests show that the SDP reformulation significantly increases the robustness of the correlation potential fitting.

We also present the comparison between the performance of SDP and least squares fitting for the 1D Hubbard model, where we observe that the success rate of SDP is 100%. These results are reported in Appendix F.

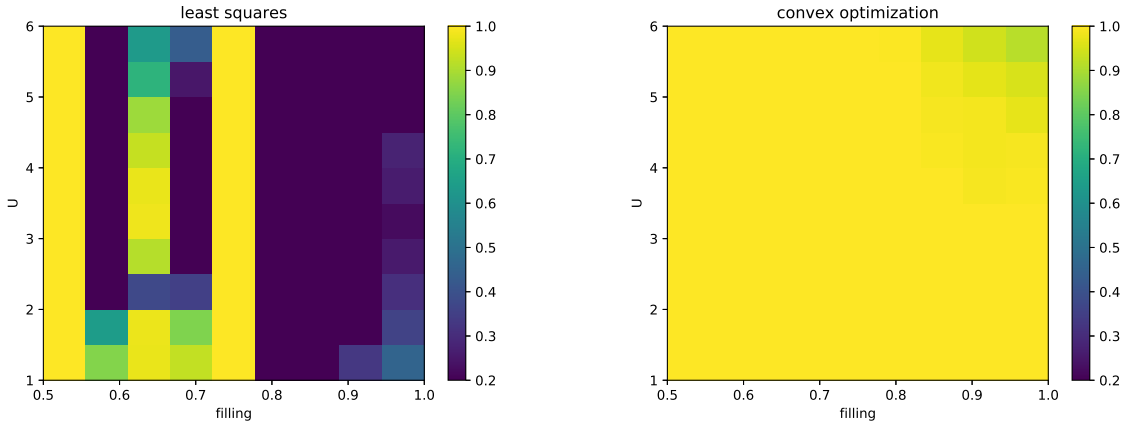


Figure 1: Success rates of the least squares (left) and convex optimization (right) approaches for 1000 samples of a 6×6 2D Hubbard model with random potential.

B. Phase diagram

For strongly-correlated systems, single-particle theories such as RHF/UHF may produce qualitatively incorrect order parameters, leading to incorrect phase diagrams. We expect that DMET/L-DMET can correct order parameters through the self-consistent iteration for the correlation potential. Without self-consistent iteration, the phase boundary of DMET/L-DMET tends to be very similar to that of UHF. As an example, we study the phase transition between antiferromagnetism and paramagnetism as studied in [33]. We impose the constraint that all impurities should be translation-invariant (TI). The TI constraint is crucial for improving the convergence behavior of DMET and L-DMET especially around the phase boundary.

We perform a series of computations on a 20×20 lattice. The fragment size is 2×2 . The filling factor n and the interaction strength U define two axes of the phase diagram. We consider 21 uniformly-spaced values of n and 26 uniformly-spaced values of U . We use the spin polarization to identify the phases. The spin polarization is defined as

$$m = \frac{|\text{Tr}(D^{\text{hl},\uparrow}) - \text{Tr}(D^{\text{hl},\downarrow})|}{\text{Tr}(D^{\text{hl},\uparrow}) + \text{Tr}(D^{\text{hl},\downarrow})}.$$

$D^{\text{hl},\uparrow}$ and $D^{\text{hl},\downarrow}$ are, respectively, the spin-up and spin-down components of the high-level global density matrices. The spin polarization as a function of n and U is presented in Fig. 2. The phase diagrams of DMET, and L-DMET are almost identical except for certain points on the phase boundary. Both are significantly different from the UHF phase diagram.

The lower-left corner of the phase diagram corresponds to gapless low-level systems, and the phase diagrams obtained from DMET and L-DMET slightly differ here. The performance of L-DMET is better than the previously proposed p-DMET method [33], which leads to a slightly blurred phase boundary.

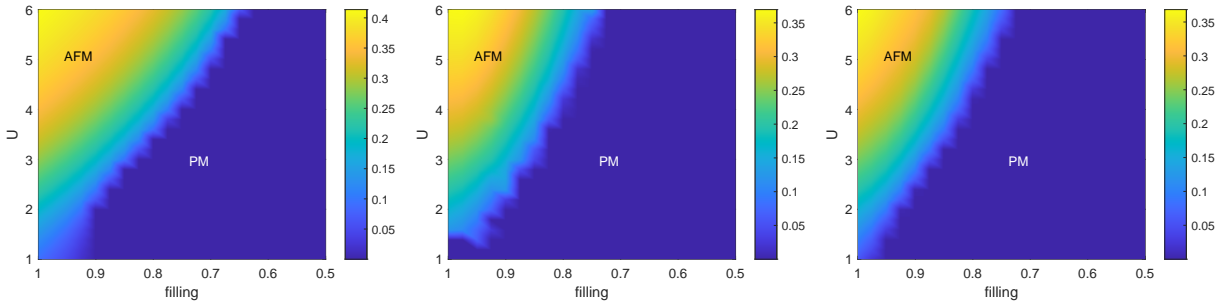


Figure 2: The comparison of phase diagrams of UHF (left), DMET (middle) and L-DMET (right) for the 2D Hubbard model. The color indicates the spin polarization.

C. Robustness with respect to the initial guess

We now demonstrate the numerical stability of the L-DMET method with respect to the initial guess. We consider two filling factors for the 6×6 2D Hubbard model at $U = 4$: filling $n = 1.0$ (36 electrons) and filling $n = 0.5$ (18 electrons), for which the solution is in the antiferromagnetic (AFM) and paramagnetic (PM) phase, respectively. For all calculations in this section, we take the fragment size to be 2×2 .

To show that L-DMET is also effective when the system is inhomogeneous, we explicitly break the translation symmetry by introducing a random on-site potential. Each entry of the random potential is sampled independently from the uniform distribution $\mathcal{U}[-0.2, 0.2]$. We deliberately choose the initial guess to have the wrong order parameter in order to test the robustness of the algorithm. We choose initial guesses for the DMET loop by incompletely converging the self-consistent field iteration for UHF (i.e., terminating after a fixed number of iterations). We in turn initialize our UHF calculations with hand-picked initial guesses; since the self-consistent iteration for UHF is terminated before convergence, the result (which we use as our initialization for DMET) depends on the initial guess.

In the AFM case ($n = 1.0$), the initial guess for UHF is chosen to be a state in the PM phase, which is obtained by alternatively adding/subtracting a small number (10^{-3}) to the

uniform density according to a checkerboard pattern. In the PM case, we initialize UHF in the AFM phase with spin-up and spin-down densities of 0.1 and 0.4 respectively. We terminate UHF after the 1st, 5th, and 10th iterations to provide initial guesses for DMET and L-DMET.

For both DMET and L-DMET, we use DIIS to accelerate the convergence starting from the second iteration. We compare the convergence of DMET and L-DMET with the same random potential in Fig. 3. Both DMET and L-DMET converge to the same fixed point within 12 iterations with different initial guesses. This experiment verifies two crucial features of L-DMET: (1) L-DMET reaches the same solution as DMET at self-consistency, when the low-level model is gapped, and (2) in both the PM phase and AFM phase, the fixed point of L-DMET is independent of the choice of the initial guess. More specially, with different unconverged UHF initial guesses, L-DMET always converges to the same fixed point as DMET does.

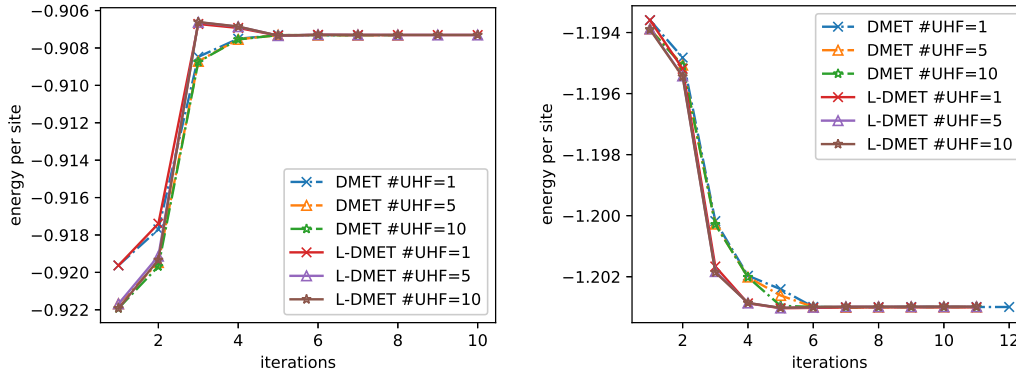


Figure 3: The convergence of the energy per site for DMET and L-DMET with different initial guesses. Results are shown for the 6×6 Hubbard model at $U = 4.0$ with fragment size 2×2 . The filling is specified by $n = 0.5$, 18 electrons (left) and $n = 1.0$, 36 electrons (right). The initialization procedure for the figures at left and right are described in the text of section VIC.

D. Jacobian of the fixed point mapping

Fig. 3 shows that the number of iterations needed for L-DMET to converge is approximately the same as for DMET, starting from a range of initial guesses. The same behavior

is also observed for all the numerical tests presented in this paper. This finding is somewhat counterintuitive, given that L-DMET updates the correlation potential only locally, while DMET can use the information of the global density matrix and update the correlation potential globally. From the perspective of solving the fixed point problem in Eq. (9), the convergence rate in the linear response regime is largely affected by the properties of the Jacobian matrix of $\mathfrak{F} \circ \mathfrak{D}$, where the mapping \mathfrak{F} stands for $\mathfrak{F}^{\text{DMET}}$ and $\mathfrak{F}^{\text{L-DMET}}$ in DMET and L-DMET, respectively.

To illustrate the properties of the Jacobian, we consider 1D Hubbard model with 24 sites with anti-periodic boundary condition. The total number of electrons is 24 (i.e., half-filling). Each fragment has 2 sites. The low-level method is the restricted Hartree-Fock method. We investigate two quantities in the self-consistent equation in Eq. (9): the linear response of $D_x^{\text{hl,frag}}$ with respect to u , i.e., $R = \partial D_x^{\text{hl,frag}} / \partial u$ and the Jacobian matrix of Eq. (9). As shown in Fig. 4 (a), the matrix R is highly localized. This means that the response of the density matrix block $D_x^{\text{hl,frag}}$ is relatively small with respect to the perturbation of the correlation potential u_y in another fragment y , when x and y are far apart from one other. Such ‘near-sighted’ dependence implies that the local update procedure can also lead to an effective iteration scheme.

Fig. 4 (b) shows that the spectral radius of the Jacobian matrix of DMET and that of L-DMET are relatively small. For the range of U ’s studied, the spectral radius is uniformly smaller than 0.2 (and in particular smaller than 1). Hence $\mathfrak{F} \circ \mathfrak{D}$ can define a contraction mapping even without mixing, and as such the fixed point problem in Eq. (9) is easy to solve. It is also interesting to observe that the spectral radius peaks around $U \approx 2.5$. For larger value of U , the spectral radius decreases with respect to U , indicating that the DMET/L-DMET iterations are easier to converge numerically.

E. Efficiency

L-DMET mainly reduces the computational cost at the single-particle level (i.e., low level). The CPU time for 2D Hubbard systems ranging from size 6×6 to 18×18 (with fragment size 2×2 in all cases) is reported in Fig. 5. We report the time of the low-level and high-level calculations separately. Each calculation is performed on a single core. The cost of the low-level calculations in DMET grows as $\mathcal{O}(L^{3.04})$, while the cost of low-level

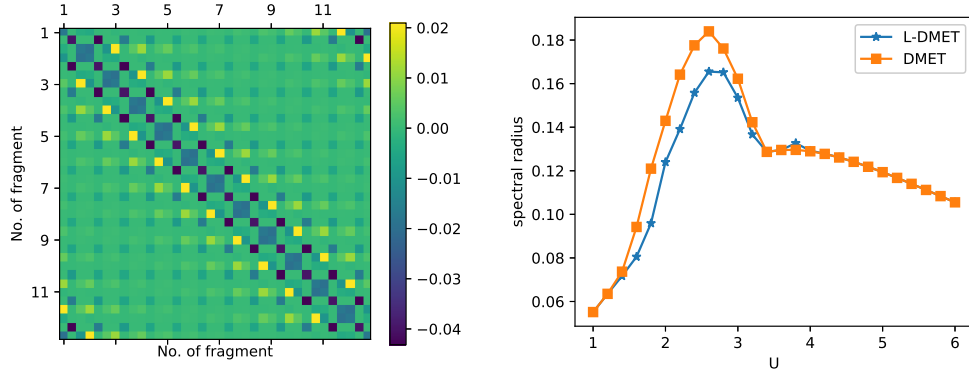


Figure 4: The matrix $\partial D^{\text{hl,frag}}/\partial u$ (left) at $U = 4.0$, and the spectral radius of the Jacobian of Eq. (9) for DMET and L-DMET (right). There are 3 degrees of freedom within u_x and $D_x^{\text{hl,frag}}$ for each fragment x ; hence the size of the matrix $\partial D^{\text{hl,frag}}/\partial u$ is 36×36 , viewed as a 12×12 matrix of 3×3 blocks.

calculation in L-DMET is reduced to $\mathcal{O}(L^{1.22})$. When the number of sites is 324, L-DMET is 49 times faster than DMET for the low-level calculations.

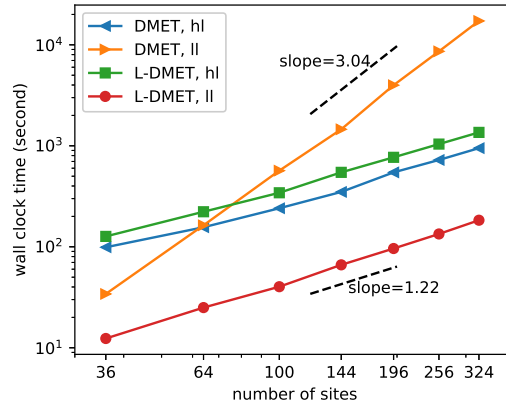


Figure 5: Computational cost of DMET and L-DMET calculations for 2D Hubbard models. The CPU time is averaged over 20 experiments.

VII. NUMERICAL EXPERIMENTS: HYDROGEN CHAIN

A. Efficiency and accuracy

In this section, we consider the application of L-DMET to a real quantum-chemical system, the hydrogen chain. The Hamiltonian is discretized using the STO-6G basis set, and these basis functions are orthogonalized with the Löwdin orthogonalization procedure. We use open boundary conditions and the restricted Hartree-Fock (RHF) method for the low-level method. The chain is partitioned into fragments with 2 adjacent atoms in each fragment, and the fragments do not overlap with each other. The high-level problem is solved with the full configuration-interaction (FCI) method. The CPU times for the low-level and the high-level parts of the calculation are aggregated separately over the entire self-consistent loop.

Fig. 6 shows that as the system size increases, the costs of both DMET and L-DMET calculations are dominated by the low-level calculations. As a result, L-DMET is significantly faster than DMET due to the acceleration of the low-level calculations. When the number of orbitals is 128 (i.e., 128 atoms), the low-level part of L-DMET is 13.5 times faster than that of DMET. Meanwhile, the wall clock times for the high-level parts of DMET and L-DMET are comparable for all systems considered.

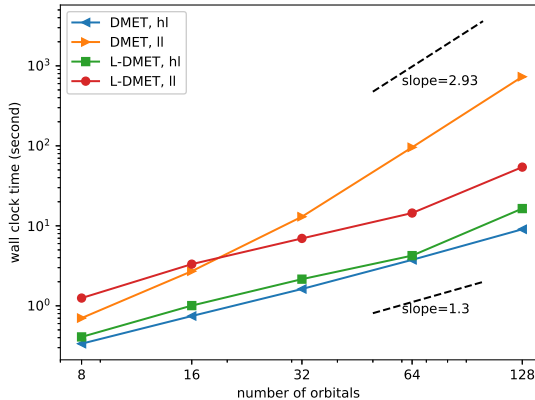


Figure 6: Computational cost of DMET and L-DMET calculations for hydrogen chains.

To demonstrate the accuracy of L-DMET, we report the dissociation energy curve for a hydrogen chain with 10 atoms. We start from an equidistant configuration and stretch the hydrogen chain, maintaining equal distances between atoms. The total energy curves of

RHF, FCI, DMET, and L-DMET are shown in Figure 7. The DMET and L-DMET curves are indistinguishable at all bond lengths. Compared to the exact value (FCI energy), the total energy errors of DMET and L-DMET are uniformly less than 0.01 a.u.

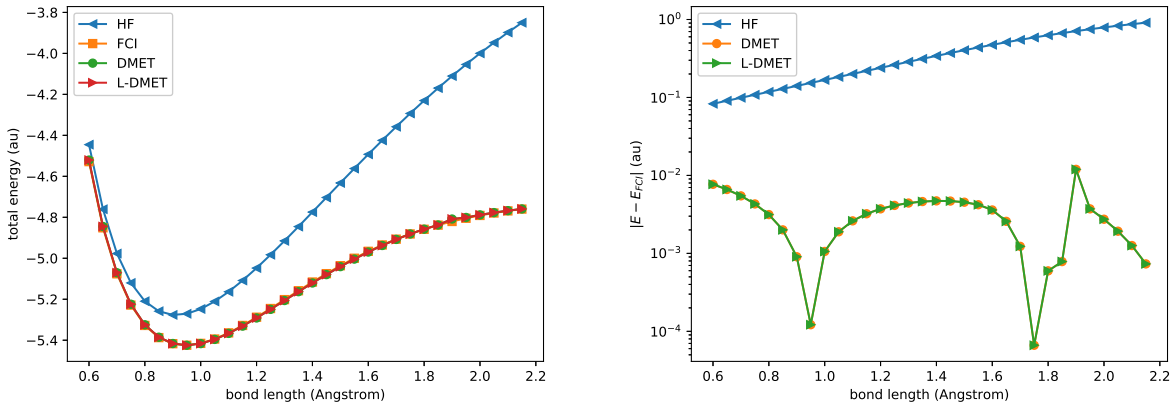


Figure 7: Total energy of the hydrogen chain as computed by HF, FCI, DMET, and L-DMET (left). Error of the total energy as computed by HF, DMET, and L-DMET (right).

B. Impact of the fragment size

To improve the accuracy of DMET calculations, one may consider increasing the fragment size. However, we demonstrate that larger fragments can lead to numerical difficulties. In particular, we observe that a large fragment size can easily lead result in a gapless low-level model, which complicates the self-consistent iterations in DMET/L-DMET calculations.

We demonstrate the issue using a hydrogen chain with 36 atoms and a bond length of 1 a.u. The coupled cluster method with singles and doubles (CCSD) is employed to solve impurity problems. We consider different partitions of the orbitals specified by fragment sizes of 1, 2, 3, 4, 6, 9, and 12. Furthermore, we experiment with multiple fitting strategies for each partitioning of the entire system by performing correlation potential fitting using possibly finer partitions of the system. For instance, when the fragment size is 6 and there are 4 fragments, we may choose to perform correlation potential fitting by considering only the diagonal blocks of size 3, so that there are 8 blocks in total. This second block size will be referred to the ‘fitting size,’ as opposed to the ‘fragment size’ which specifies the size of

the impurity problems that are solved. Note that the fragment size must be a multiple of the fitting size. When the fitting size is 1, DMET reduces to the density embedding theory (DET)[18]. According to Appendix A, when the fitting size is too large, the correlation potential may not be unique.

As shown in Figure 8, when the fitting size is set to be the same as the fragment size in DMET, the gap of the low-level Hamiltonian decreases as the fragment size increases. It eventually vanishes when the fragment size is greater than 6. However, if we fix the fitting size, the gap tends to be a constant as the fragment size increases. The same observations apply for L-DMET. Different fitting sizes also lead to different convergence patterns of the total energy as the fragment size increases. After enough iterations, the total energies computed with different fitting sizes become comparable, but we observe that the DMET and L-DMET self-consistent iterations are more stable when the low-level energy gap does not vanish.

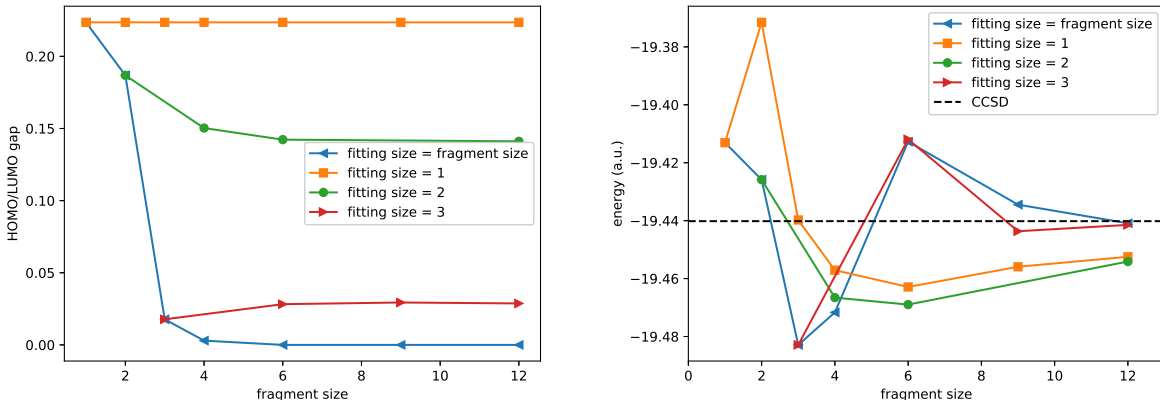


Figure 8: Low-level HOMO-LUMO gap (left) and total DMET energy (right) for different fragment sizes and fitting sizes. The dotted line (right) shows the CCSD energy for the entire system as a reference.

VIII. CONCLUSION

In this paper, we propose the L-DMET method for tackling the problem of correlation potential fitting in the density matrix embedding theory (DMET). This is often a computational bottleneck in large-scale DMET calculations, particularly for inhomogeneous systems.

L-DMET improves the robustness of the correlation potential fitting using an approach that relies on convex optimization—in particular, semidefinite programming (SDP). The SDP reformulation allows us to provably find the correlation potential, when the correlation potential is uniquely defined. It also allows us to use state-of-the-art numerical methods and software packages to compute the correlation potential in a robust fashion. Meanwhile, L-DMET improves the efficiency of the correlation potential fitting by replaces the global fitting procedure with several local correlation potential fitting procedures for each fragment. Moreover, we have shown that under certain natural conditions, the fixed points of L-DMET coincide with the original DMET. We demonstrate the accuracy, efficiency, and robustness of the L-DMET method by testing on Hubbard models and the hydrogen chain.

The question of whether the correlation potential is uniquely defined is central to both DMET and L-DMET. We show that in order to obtain a unique correlation potential, a necessary condition is that $N_e \geq L_A$, i.e., that the total electron number is larger than the fragment size. In practice we observe that the correlation potential is indeed often (but not always) unique when $N_e \geq L_A$. We remark that the issue of finding a unique correlation potential is particularly relevant now due to the recent progress of *ab initio* DMET calculations [20], where the fragment size can be large due to the use of a large basis set. Hence a rigorous understanding of sufficient conditions for the uniqueness of the correlation potential, as well as practical remedies when the correlation potential fails to be unique, are important issues that we shall consider in future work.

ACKNOWLEDGMENTS:

This work was partially supported by the Air Force Office of Scientific Research under award number FA9550-18-1-0095 (X.W., M.L., Y.T., L.L.), by the Department of Energy under Grant No. DE-SC0017867 (X.W. and L.L.), by the Department of Energy CAMERA program (Y.T. and L.L.), by the National Science Foundation Graduate Research Fellowship Program under grant DGE-1106400 (M.L.), and by the National Science Foundation under Award No. 1903031 (M.L.). We thank Berkeley Research Computing (BRC), Google Cloud Platform (GCP), and National Energy Research Scientific Computing Center (NERSC) for

computing resources. We thank Garnet Chan for helpful discussions.

- [1] Knowles, P. J.; Handy, N. C. A new determinant-based full configuration interaction method. *Chemical Physics Letters* **1984**, *111*, 315–321.
- [2] Olsen, J.; Jørgensen, P.; Simons, J. Passing the one-billion limit in full configuration-interaction (FCI) calculations. *Chemical Physics Letters* **1990**, *169*, 463–472.
- [3] Vogiatzis, K. D.; Ma, D.; Olsen, J.; Gagliardi, L.; de Jong, W. A. Pushing configuration-interaction to the limit: Towards massively parallel MCSCF calculations. *The Journal of chemical physics* **2017**, *147*, 184111.
- [4] Lin, H. Exact diagonalization of quantum-spin models. *Physical Review B* **1990**, *42*, 6561.
- [5] Läuchli, A. M.; Sudan, J.; Sørensen, E. S. Ground-state energy and spin gap of spin-1 2 Kagomé-Heisenberg antiferromagnetic clusters: Large-scale exact diagonalization results. *Physical Review B* **2011**, *83*, 212401.
- [6] White, S. R. Density Matrix Formulation for Quantum Renormalization Groups. *Phys. Rev. Lett.* **1992**, *69*, 2863–2866.
- [7] Sun, Q.; Chan, G. K.-L. Quantum embedding theories. *Accounts of Chemical Research* **2016**, *49*, 2705–2712.
- [8] Imada, M.; Miyake, T. Electronic structure calculation by first principles for strongly correlated electron systems. *Journal of the Physical Society of Japan* **2010**, *79*, 112001.
- [9] Ayral, T.; Lee, T.-H.; Kotliar, G. Dynamical mean-field theory, density-matrix embedding theory, and rotationally invariant slave bosons: A unified perspective. *Physical Review B* **2017**, *96*, 235139.
- [10] Metzner, W.; Vollhardt, D. Correlated lattice fermions in $d = \infty$ dimensions. *Physical Review Letters* **1989**, *62*, 324.
- [11] Georges, A.; Krauth, W. Numerical solution of the $d = \infty$ Hubbard model: Evidence for a Mott transition. *Physical Review Letters* **1992**, *69*, 1240.
- [12] Georges, A.; Kotliar, G.; Krauth, W.; Rozenberg, M. J. Dynamical mean-field theory of strongly correlated fermion systems and the limit of infinite dimensions. *Reviews of Modern Physics* **1996**, *68*, 13.

- [13] Kotliar, G.; Savrasov, S. Y.; Haule, K.; Oudovenko, V. S.; Parcollet, O.; Marianetti, C. Electronic structure calculations with dynamical mean-field theory. *Reviews of Modern Physics* **2006**, *78*, 865.
- [14] Zhu, T.; Cui, Z.-H.; Chan, G. K.-L. Efficient Formulation of Ab Initio Quantum Embedding in Periodic Systems: Dynamical Mean-Field Theory. *Journal of Chemical Theory and Computation* **2019**,
- [15] Knizia, G.; Chan, G. K.-L. Density matrix embedding: A simple alternative to dynamical mean-field theory. *Physical Review Letters* **2012**, *109*, 186404.
- [16] Knizia, G.; Chan, G. K.-L. Density matrix embedding: A strong-coupling quantum embedding theory. *Journal of Chemical Theory and Computation* **2013**, *9*, 1428–1432.
- [17] Tsuchimochi, T.; Welborn, M.; Van Voorhis, T. Density matrix embedding in an antisymmetrized geminal power bath. *The Journal of Chemical Physics* **2015**, *143*, 024107.
- [18] Bulik, I. W.; Scuseria, G. E.; Dukelsky, J. Density matrix embedding from broken symmetry lattice mean fields. *Physical Review B* **2014**, *89*, 035140.
- [19] Wouters, S.; Jiménez-Hoyos, C. A.; Sun, Q.; Chan, G. K.-L. A practical guide to density matrix embedding theory in quantum chemistry. *Journal of Chemical Theory and Computation* **2016**, *12*, 2706–2719.
- [20] Cui, Z.-H.; Zhu, T.; Chan, G. K.-L. Efficient Implementation of Ab Initio Quantum Embedding in Periodic Systems: Density Matrix Embedding Theory. *Journal of Chemical Theory and Computation* **2019**,
- [21] Sun, C.; Ray, U.; Cui, Z.-H.; Stoudenmire, M.; Ferrero, M.; Chan, G. K. Finite temperature density matrix embedding theory. *arXiv preprint arXiv:1911.07439* **2019**,
- [22] Cui, Z.-H.; Sun, C.; Ray, U.; Zheng, B.-X.; Sun, Q.; Chan, G. K. Ground-state phase diagram of the three-band Hubbard model in various parametrizations from density matrix embedding theory. *arXiv preprint arXiv:2001.04951* **2020**,
- [23] Chen, Q.; Booth, G. H.; Sharma, S.; Knizia, G.; Chan, G. K.-L. Intermediate and spin-liquid phase of the half-filled honeycomb Hubbard model. *Physical Review B* **2014**, *89*, 165134.
- [24] Zheng, B.-X.; Chan, G. K.-L. Ground-state phase diagram of the square lattice Hubbard model from density matrix embedding theory. *Physical Review B* **2016**, *93*, 035126.
- [25] Zheng, B.-X.; Kretchmer, J. S.; Shi, H.; Zhang, S.; Chan, G. K.-L. Cluster size convergence of the density matrix embedding theory and its dynamical cluster formulation: A study with

- an auxiliary-field quantum Monte Carlo solver. *Physical Review B* **2017**, *95*, 045103.
- [26] Zheng, B.-X.; Chung, C.-M.; Corboz, P.; Ehlers, G.; Qin, M.-P.; Noack, R. M.; Shi, H.; White, S. R.; Zhang, S.; Chan, G. K.-L. Stripe order in the underdoped region of the two-dimensional Hubbard model. *Science* **2017**, *358*, 1155–1160.
- [27] Fan, Z.; Jie, Q.-l. Cluster density matrix embedding theory for quantum spin systems. *Physical Review B* **2015**, *91*, 195118.
- [28] Gunst, K.; Wouters, S.; De Baerdemacker, S.; Van Neck, D. Block product density matrix embedding theory for strongly correlated spin systems. *Physical Review B* **2017**, *95*, 195127.
- [29] Pham, H. Q.; Bernales, V.; Gagliardi, L. Can Density Matrix Embedding Theory with the Complete Activate Space Self-Consistent Field Solver Describe Single and Double Bond Breaking in Molecular Systems? *Journal of Chemical Theory and Computation* **2018**, *14*, 1960–1968.
- [30] Jensen, D. S.; Wasserman, A. Numerical methods for the inverse problem of density functional theory. *Int. J. Quantum Chem.* **2017**, *118*, e25425.
- [31] Wu, Q.; Yang, W. A direct optimization method for calculating density functionals and exchange–correlation potentials from electron densities. *J. Chem. Phys.* **2003**, *118*, 2498.
- [32] Baroni, S.; de Gironcoli, S.; Dal Corso, A.; Giannozzi, P. Phonons and related crystal properties from density-functional perturbation theory. *Rev. Mod. Phys.* **2001**, *73*, 515–562.
- [33] Wu, X.; Cui, Z.-H.; Tong, Y.; Lindsey, M.; Chan, G. K.-L.; Lin, L. Projected Density Matrix Embedding Theory with Applications to the Two-Dimensional Hubbard Model. *J. Chem. Phys.* **2019**, *151*, 064108.
- [34] Van Loan, C. Computing the CS and the generalized singular value decompositions. *Numer. Math.* **1985**, *46*, 479–491.
- [35] Golub, G. H.; Van Loan, C. F. *Matrix computations*, 4th ed.; Johns Hopkins Univ. Press: Baltimore, 2013.
- [36] Rockafellar, R. T. *Convex analysis*; Princeton University Press, 1970.
- [37] Lieb, E. H. Density functional for Coulomb systems. *Int J. Quantum Chem.* **1983**, *24*, 243.
- [38] Onari, S.; Arita, R.; Kuroki, K.; Aoki, H. Phase diagram of the two-dimensional extended Hubbard model: Phase transitions between different pairing symmetries when charge and spin fluctuations coexist. *Phys. Rev. B* **2004**, *70*, 094523.

- [39] Dahm, T.; Manske, D.; Tewordt, L. Charge-density-wave and superconductivity d -wave gaps in the Hubbard model for underdoped high- T_c cuprates. *Phys. Rev. B* **1997**, *56*, R11419–R11422.
- [40] Kato, M.; Machida, K.; Nakanishi, H.; Fujita, M. Soliton Lattice Modulation of Incommensurate Spin Density Wave in Two Dimensional Hubbard Model -A Mean Field Study-. *Journal of the Physical Society of Japan* **1990**, *59*, 1047–1058.
- [41] Mizusaki, T.; Imada, M. Gapless quantum spin liquid, stripe, and antiferromagnetic phases in frustrated Hubbard models in two dimensions. *Physical Review B* **2006**, *74*, 014421.
- [42] O’Donoghue, B.; Chu, E.; Parikh, N.; Boyd, S. Conic Optimization via Operator Splitting and Homogeneous Self-Dual Embedding. *Journal of Optimization Theory and Applications* **2016**, *169*, 1042–1068.
- [43] O’Donoghue, B.; Chu, E.; Parikh, N.; Boyd, S. SCS: Splitting Conic Solver, version 2.1.1. <https://github.com/cvxgrp/scs>, 2017.
- [44] Diamond, S.; Boyd, S. CVXPY: A Python-Embedded Modeling Language for Convex Optimization. *Journal of Machine Learning Research* **2016**, *17*, 1–5.
- [45] Agrawal, A.; Verschueren, R.; Diamond, S.; Boyd, S. A Rewriting System for Convex Optimization Problems. *Journal of Control and Decision* **2018**, *5*, 42–60.

Appendix A: Uniqueness of the correlation potential

Here we demonstrate that the condition $N_e \geq L_A$ as in Assumption 1 is necessary for the correlation potential to be unique. Suppose $N_e < L_A$ and there exists $u \in \mathcal{S}^0$ such that $f + u$ is gapped. Then let u_1, \dots, u_{N_e} be eigenvectors of $f + u$ spanning the occupied subspace, so that $D := \mathcal{D}(f + u, N_e) = \sum_{i=1}^{N_e} u_i u_i^*$. Then let $v_1^x, \dots, v_{N_e}^x \in \mathbb{C}^{L_A}$ be defined via $v_i^x = (\Phi_x^{\text{frag}})^\dagger u_i$ as the components of the u_i within an arbitrary fragment x . Since $N_e < L_A$, there exists some vector $w^x \in \mathbb{C}^{L_A}$ with $\|w^x\| = 1$ which is orthogonal to all of the v_i^x . Let $W = (\Phi_x^{\text{frag}})(w^x)(w^x)^\dagger(\Phi_x^{\text{frag}})^\dagger$. Then by construction, all the u_i are in the null space of W for $i = 1, \dots, N_e$. Hence the u_i are eigenvectors of $f + u + \tau(W - I)$ for $i = 1, \dots, N_e$, all $\tau \in \mathbb{R}$. Note that $\tau(W - I) \in \mathcal{S}^0$, and since $f + u$ is gapped, when τ is sufficiently small, we have $\mathcal{D}(f + u + \tau(W - I), N_e) = \sum_{i=1}^{N_e} u_i u_i^* = D$, contradicting uniqueness.

Appendix B: Obtaining bath orbitals from the low-level density matrix

The global low-level density matrix, obtained from the decomposition in Eq. (4) takes the form

$$D^{\text{ll}} = \begin{pmatrix} U_A \Sigma_A^2 U_A^\dagger & U_A \Sigma_A \Sigma_B U_B^\dagger \\ U_B \Sigma_B \Sigma_A U_A^\dagger & U_B \Sigma_B^2 U_B^\dagger + U_{\text{core}} U_{\text{core}}^\dagger \end{pmatrix} := \begin{pmatrix} D_{11} & D_{12} \\ D_{21} & D_{22} \end{pmatrix}. \quad (\text{B1})$$

where D_{11} corresponds to the fragment x only. Then the CS decomposition (4), and hence the bath and core orbitals can also be identified from D^{ll} directly. The eigenvalue decomposition of D_{11} directly gives

$$D_{11} = U_A \Sigma_A^2 U_A^\dagger. \quad (\text{B2})$$

The bath-fragment density matrix can be written as

$$D_{21} = C_B C_A^\dagger = U_B \Sigma_B \Sigma_A U_A^\dagger. \quad (\text{B3})$$

The unitary matrix U_B can be calculated by normalizing all the columns of the matrix $D_{21} U_A$, since

$$U_B \Sigma_B \Sigma_A = D_{21} U_A.$$

The diagonal elements of $\Sigma_A \Sigma_B$ are the corresponding norms of the columns. As a result, Σ_B is also obtained with the known Σ_A in (B2). Therefore we obtain the bath orbitals. Once the bath orbitals are obtained, the core orbitals can be obtained from the following relation

$$U_{\text{core}} U_{\text{core}}^\dagger = D_{22} - U_B \Sigma_B^2 U_B^\dagger. \quad (\text{B4})$$

Appendix C: Proof of Proposition 2

Heuristically, the idea for proving Proposition 2 is that the first-order optimality conditions for the optimization problem of Eq. (10) (assuming differentiability at the optimizer) are precisely $\nabla_{u_x} F(u) = D_x^{\text{hl,frag}}$, i.e., equivalent to exact fitting. However, some care is required when F is singular at the optimizer.

We think of F as a function on (N_f) -tuples of $L_A \times L_A$ (Hermitian) matrices $(u_x)_{x=1}^{N_f} = (u_1, \dots, u_{N_f})$. This domain is identified with \mathcal{S} as a slight abuse of notation. As above we denote $u = \bigoplus_{x=1}^{N_f} u_x$, but by some abuse of notation we will also identify u with $(u_x)_{x=1}^{N_f} = (u_1, \dots, u_{N_f})$.

Since we are given diagonal blocks $D_x^{\text{hl,frag}}$ that we want to fit by choice of correlation potential blocks u_x , we want to invert the gradient of F . We roughly understand that the gradient of $\nabla F = (\nabla_{u_x} F)_{x=1}^{N_f}$ is invertible (up to shifting by a scalar matrix), with inverse specified by the gradient of the concave conjugate or Legendre-Fenchel transform F^* . But since F is not differentiable everywhere, in fact the *supergradient* [36] mapping ∂F must be considered. Under this mapping, each singular point $(u_x)_{x=1}^{N_f}$ of F maps to all $(P_x)_{x=1}^{N_f}$ lying in the supergradient set of F at $(u_x)_{x=1}^{N_f}$, i.e., all $(P_x)_{x=1}^{N_f}$ such that

$$F(v) \leq F(u) + \sum_x \text{Tr}[P_x(v_x - u_x)]$$

for all $v \in S$.

The set of optimizers of (10) is precisely the set $\partial F^*(P)$ [36]. Moreover we have $P \in \partial F(u)$ if and only if $u \in \partial F^*(P)$ [36]. Hence provided that P is in the supergradient image of F , the set of optimizers of (10) is nonempty, and any element u^* satisfies $P \in \partial F(u^*)$. Moreover, if $f + u^*$ is gapped, then as previously discussed F is differentiable at u^* , i.e., the subgradient is a singleton, and $\nabla F(u^*) = P$, i.e., u^* attains exact fitting according to P . Finally, if u^* is the unique optimizer, then it follows that there does not exist $u \neq u^*$ such that $P \in \partial F(u)$. Hence if u^* is the unique optimizer and $f + u^*$ is gapless, then there is no correlation potential yielding an exact fit.

Then to complete the proof it suffices to show that our assumptions on $(D_x^{\text{hl,frag}})_{x=1}^{N_f}$ (i.e., that $0 \prec D_x^{\text{hl,frag}} \prec I_{L_A}$ and $\sum_x \text{Tr}[D_x^{\text{hl,frag}}] = N_e$) imply that $(D_x^{\text{hl,frag}})_{x=1}^{N_f}$ lies in the supergradient image of F . To understand the supergradient image of F and how to construct the correlation potential u more explicitly, we must study the concave conjugate F^* .

Recall that the effective domain $\text{dom}(F^*)$ of F^* is defined as the set of all points for which $F^* > -\infty$. The relative interior (i.e., the interior of the effective domain within its affine hull [36]) of the effective domain coincides with the supergradient image of F [36], so we want to understand it.

To this end we shall concoct an alternate formula for F^* . First recall that $F^{**} = F$, i.e.,

$$F(u) = \inf_{(P_x)_{x=1}^{N_f} \in \text{dom}(F^*)} \left\{ \sum_{x=1}^{N_f} \text{Tr}[P_x u_x] - F^*(P_1, \dots, P_{N_f}) \right\}.$$

Meanwhile observe that for A Hermitian,

$$\mathcal{E}_{N_e}(A) = \inf \{ \text{Tr}[AP] : 0 \preceq P \preceq I_L, \text{Tr}[P] = N_e \},$$

so applying this result to $F(u) = \mathcal{E}_{N_e}(f + u)$, we see that

$$\begin{aligned} F(u) &= \mathcal{E}_{N_e}(f + u) \\ &= \inf_{P^\dagger=P} \left\{ \sum_{x=1}^{N_f} \text{Tr}[P_x u_x] - G(P) \right\} \\ &= \inf_{(P_x) \text{ Hermitian}} \left\{ \sum_{x=1}^{N_f} \text{Tr}[P_x u_x] - \sup_{P: P_x=[P]_x \forall x} G(P) \right\} \end{aligned}$$

where

$$G(P) = \begin{cases} -\text{Tr}[tP], & 0 \preceq P \preceq I_L, \text{Tr}[P] = N_e \\ -\infty, & \text{otherwise.} \end{cases}$$

But consequently $F = g^*$, where

$$g(P_1, \dots, P_{N_f}) = \sup_{P: P_x=[P]_x \forall x} G(P) = - \inf_{0 \preceq P \preceq I_L: \text{Tr}[P]=N_e, [P]_x=P_x \forall x} \text{Tr}[tP].$$

Then it its clear that

$$\text{dom}(F^*) = \left\{ (P_1, \dots, P_{N_f}) : 0 \preceq P_x \preceq I_{L_A} \text{ for } x = 1, \dots, N_f, \sum_{x=1}^{N_f} \text{Tr}[P_x] = N_e \right\}.$$

Hence the relative interior of the effective domain is given by

$$\text{relint dom}(F^*) = \left\{ (P_1, \dots, P_{N_f}) : 0 \prec P_x \prec I_{L_A} \text{ for } x = 1, \dots, N_f, \sum_{x=1}^{N_f} \text{Tr}[P_x] = N_e \right\}.$$

Our assumption on $(D_x^{\text{hl,frag}})_{x=1}^{N_f}$ was precisely that it lies in this set, so $(D_x^{\text{hl,frag}})_{x=1}^{N_f}$ lies in the supergradient image of F , and the proof is complete.

Appendix D: Proof of Proposition 3

Recall that for fixed $P = (P_1, \dots, P_{N_f})$ satisfying $0 \prec P_x \preceq I_{L_A}$ for all x and $\sum_x \text{Tr}[P_x] = N_e$, we want to solve

$$\inf_{u \in S^0} \left[\sum_x \text{Tr}[P_x u_x] - F(u) \right].$$

Recall that

$$F(u) = F(u_1, \dots, u_{N_f}) = \mathcal{E}_{N_e}[h + u],$$

and \mathcal{E}_{N_e} indicates sum of lowest N_e eigenvalues. We will write $F(u)$ as the optimal value of a suitable concave maximization problem and plug this into the above convex minimization problem to derive an SDP equivalent to what we want to solve.

First we observe that for any symmetric A and any m , we can write $\mathcal{E}_m(A)$ as the optimal value of the convex *minimization* problem:

$$\mathcal{E}_m(A) = \inf \{ \text{Tr}(AX) : \text{Tr}(X) = m, 0 \preceq X \preceq I \}.$$

Then we will derive the dual of this minimization problem to write $\mathcal{E}_m(A)$ as the optimal value of a concave maximization problem. To wit, write the Lagrangian,

$$\begin{aligned} \mathcal{L}(X, Y, Z, \alpha) &= \text{Tr}(AX) - \text{Tr}(YX) - \text{Tr}(Z[I - X]) - \alpha(\text{Tr}(X) - m) \\ &= \text{Tr}([A - Y + Z - \alpha I]X) + \alpha m - \text{Tr}(Z) \end{aligned}$$

where the domain is defined by X symmetric, $Y \succeq 0$, $Z \succeq 0$, $\alpha \in \mathbb{R}$. Then carry out the minimization over X to derive the dual problem

$$\begin{array}{ll} \underset{Y \succeq 0, Z \succeq 0, \alpha \in \mathbb{R}}{\text{maximize}} & \alpha m - \text{Tr}(Z) \\ \text{subject to} & A - Y + Z - \alpha I \succeq 0. \end{array}$$

Evidently it is optimal to choose $Y = 0$, hence we have the equivalent program

$$\begin{array}{ll} \underset{Z \succeq 0, \alpha \in \mathbb{R}}{\text{maximize}} & \alpha m - \text{Tr}(Z) \\ \text{subject to} & A + Z - \alpha I \succeq 0. \end{array}$$

The optimal value is equal to $\mathcal{E}_m(A)$ by strong duality, i.e., we can write

$$\mathcal{E}_m(A) = \max \{ \alpha m - \text{Tr}(Z) : A + Z - \alpha I \succeq 0, Z \succeq 0, \alpha \in \mathbb{R} \}.$$

Applying this result for $A = h + u$, we see that we can rephrase our original optimization problem as

$$\begin{array}{ll} \underset{u \in S^0, Z \in \mathbb{C}^{M \times M} \text{ Hermitian}, \alpha \in \mathbb{R}}{\text{minimize}} & \sum_{x=1}^{N_f} \text{Tr}[P_x u_x] - \alpha N_e + \text{Tr}(Z) \\ \text{subject to} & h + u + Z - \alpha I \succeq 0 \\ & Z \succeq 0., \end{array}$$

as was to be shown.

Appendix E: Proof of Proposition 4

We first consider a fixed point of DMET denoted by u^* , which solves Eq. (9) with $\mathfrak{F} = \mathfrak{F}^{\text{DMET}}$. Then for any x

$$D_x^{\text{hl,frag}} = E^\top \Phi_x^\dagger \mathcal{D}(f + u^*, N_e) \Phi_x E,$$

where as before $E = (I_{L_A}, 0_{L_A \times L_A})^\top$. If we can further show that for any x ,

$$E^\top \Phi_x^\dagger \mathcal{D}(f + u^*, N_e) \Phi_x E = E^\top \mathcal{D}(\Phi_x^\dagger (f + u^*) \Phi_x, L_A) E. \quad (\text{E1})$$

then by the uniqueness of the local correlation fitting we have $\tilde{u}_x = 0$. Therefore u^* is a fixed point problem of the L-DMET.

Without loss of generality, we assume fragment x consists of orbitals $\{1, 2, \dots, L_A\}$. Using the notation in Eq. (4), the basis transformation matrix is

$$U = \begin{pmatrix} I & 0 & 0 & 0 \\ 0 & U_B & U_{\text{core}} & U_{\text{vir}} \end{pmatrix} \in \mathbb{C}^{L \times L}.$$

It can be obtained via

$$\underset{C \in \mathbb{C}^{L \times N_e}, C^\dagger C = I_{N_e}}{\text{minimize}} \quad \text{Tr}[C^\dagger (f + u^*) C], \quad (\text{E2})$$

and with respect to the new basis defined by U , Eq. (E2) becomes

$$\underset{\tilde{X} \in \mathbb{C}^{L \times N_e}, \tilde{X}^\dagger \tilde{X} = I_{N_e}}{\text{minimize}} \quad \text{Tr}[\tilde{X}^\dagger U^\dagger (f + u^*) U \tilde{X}]. \quad (\text{E3})$$

Using the decomposition (4), we have

$$\tilde{X} = U^\dagger C = \begin{pmatrix} U_A \Sigma_A V^\dagger \\ \Sigma_B V^\dagger \\ V_\perp^\dagger \\ 0 \end{pmatrix}. \quad (\text{E4})$$

Now we constrain \tilde{X} to take a more general form

$$\tilde{X} = \begin{pmatrix} X V^\dagger \\ V_\perp^\dagger \\ 0 \end{pmatrix} \in \mathbb{C}^{L \times N_e},$$

where $X \in \mathbb{C}^{2L_A \times L_A}$ and $X^\dagger X = I_{L_A}$. Then we have

$$\text{Tr}[\tilde{X}^\dagger U^\dagger (f + u^*) U \tilde{X}] = \text{Tr}[X^\dagger \Phi_x^\dagger (f + u^*) \Phi_x X] + \text{Tr}[V_\perp^\dagger \Xi V_\perp],$$

where Ξ is the diagonal matrix consisting of the eigenvalues of core orbitals. Since the second term on the right hand side does not depend on X , then $X = \begin{pmatrix} U_A \Sigma_A \\ \Sigma_B \end{pmatrix}$ solves the following minimization problem

$$\underset{X \in \mathbb{C}^{2L_A \times L_A}, X^\dagger X = I_{L_A}}{\text{minimize}} \quad \text{Tr} X^\dagger \Phi_x^\dagger (f + u^*) \Phi_x X$$

Therefore

$$E^\top \mathcal{D}(\Phi_x^\dagger (f + u^*) \Phi_x, L_A) E = E^\top X X^\dagger E = U_A \Sigma_A^2 U_A^\dagger = E^\top \Phi_x^\dagger \mathcal{D}(f + u, N_e) \Phi_x E.$$

The last equality follows from Eq. (B1).

Similarly if u^* is a fixed point of L-DMET, by Eq. (E1) it is also a fixed point of DMET.

Appendix F: Comparison of semidefinite programming and least squares fitting in 1D Hubbard model

To further evaluate the comparison between the SDP and least squares fitting, we repeat the analysis of their success rates following exactly the same procedure as outlined in section VIA, except that we now instead consider a 1D Hubbard model. In particular, we consider a 1D Hubbard chain of 40 sites with anti-periodic boundary condition, and we take fragments consisting of 2 sites. As shown in Fig. 9, the least squares approach clearly performs better than it does on the 2D Hubbard Model. Nonetheless, the least squares frequently fails when the number of electrons is 24, 28, 32, 36 and 40. Meanwhile, the SDP approach enjoys a 100% success rate on our test cases. The experiment for the 1D Hubbard model indicates again the SDP approach is more robust than the least squares approach.

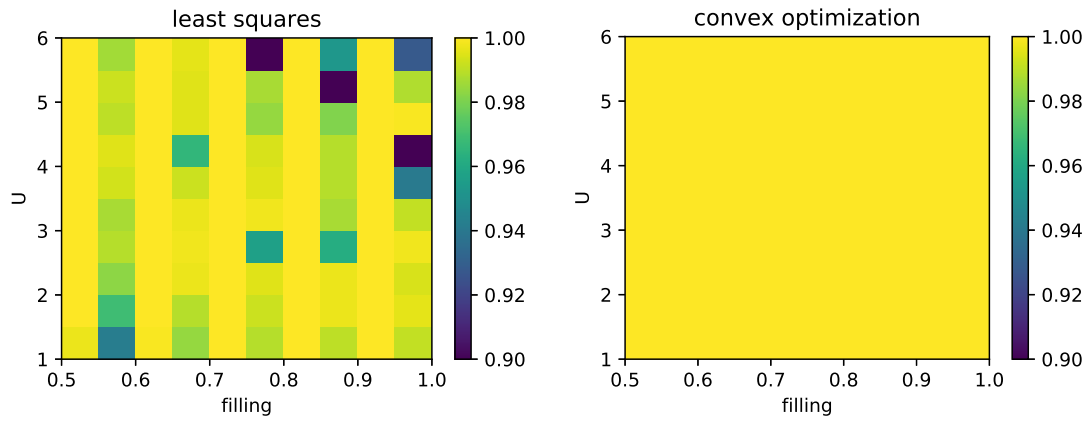


Figure 9: Success rates of the least squares (left) and convex optimization (right) approaches for the 1D Hubbard model.